

Full length article

Optical vortices in beam propagation through a self-defocussing medium

G.S. McDonald, K.S. Syed¹ and W.J. Firth

Department of Physics and Applied Physics, University of Strathclyde, 107 Rottenrow, Glasgow G4 0NG, UK

Received 21 April 1992

We present numerical simulations and analysis of optical vortex propagation in a 3D self-defocussing medium. On plane wave background initial conditions composed of points and lines of phase discontinuity are shown, in some cases, to evolve towards a regular crystal of fully nonlinear vortices. In other cases the solution more resembles a vortex gas. For gaussian beams, we have derived a simple set of ordinary differential equations which are shown to accurately describe the motion of a single vortex while the background beam undergoes significant spreading.

1. Introduction

The study of transverse effects in nonlinear optics has been mostly confined to one transverse dimension [1]. Here we study the three-dimensional nonlinear Schrödinger equation (3D NLS) which models diffraction occurring in both transverse dimensions and a medium nonlinearity that is due to the Kerr effect [2]. It is essential to consider such simple forms of nonlinearity to understand phenomena which may occur when higher order effects are later taken into account.

In propagation through self-focussing media filamentation instabilities are well known. Much current research [3–5] examines the case where the nonlinearity is self-defocussing and seeks any 3D manifestation of the 2D dark soliton [6] solution. We have shown that dark “soliton stripe” solutions of the 3D NLS may break up into rows of optical vortices when subject to perturbations of either sinusoidal or random nature [7]. At the “core” of each of these vortices the lines of zero real and imaginary parts of the field meet to form a zero in the intensity – where the phase is undefined. Circumnavigating one of these zeroes, in a counterclockwise direction, a $+$ or -2π

phase shift is picked up denoting a “topological charge” of $+1$ or -1 .

Since the dark solutions are unstable one seeks fully nonlinear structures in the plane which are robust. The existence of vortex solutions (defects) to 3D NLS-type equations has been known for some time [8]. Only recently have such phenomena been considered in nonlinear optics where, most notably, the optical vortex solutions of systems based on the laser Maxwell–Bloch equations have been studied [9,10]. The dynamics of a reduced system (in which the electric field is projected onto a *finite* basis of transverse cavity modes) has revealed stationary “crystals” of phase singularities and, in the same work, experimental confirmation has been attained [11]. These particular works were under uniform-field assumptions implying, essentially, no propagation effects. We address here the more fundamental configuration involving merely diffraction through a self-defocussing Kerr medium.

2. Vortices on gaussian beams

The 3D NLS may be conveniently scaled in the following manner to describe evolution of the electric field, F , during propagation in the z direction:

¹ Present address: Department of Physics, Imperial College, London SW7 2AZ, UK.

$$i \frac{\partial F}{\partial z} + \frac{\alpha}{2} \left(\frac{\partial^2 F}{\partial x^2} + \frac{\partial^2 F}{\partial y^2} \right) + \eta |F|^2 F = 0. \quad (1)$$

α defines the scale of the transverse plane (x - y) and, for definiteness, we choose $\eta = 1$ for a self-focussing medium and $\eta = -1$ in the self-defocussing case.

Having already proposed a method for the creation of vortices [7], we now wish to examine the characteristics of their propagation when seeded on gaussian beams.

The first and most simple initial value consideration is that of a vortex centred on a beam at the entry face of the medium. For this we consider

$$F(r, \theta, z=0) = F_0 \exp(-r^2) r \exp(im\theta), \quad (2)$$

where (r, θ) are polar coordinates in the transverse plane. The first factors simply define a gaussian profile while the latter two force a singularity in the field at beam centre which has a topological charge m .

It is instructive to ascertain precisely which features of the subsequent propagation can be attributed to nonlinear effects. For comparison we first show the resulting pattern after a length of purely linear (diffractive) propagation. In fig. 1 we show the transverse intensity profile of the beam at $z = 50$. One can see that the defect seed merely forms a wide ring in the far field, indeed the pattern simply approaches

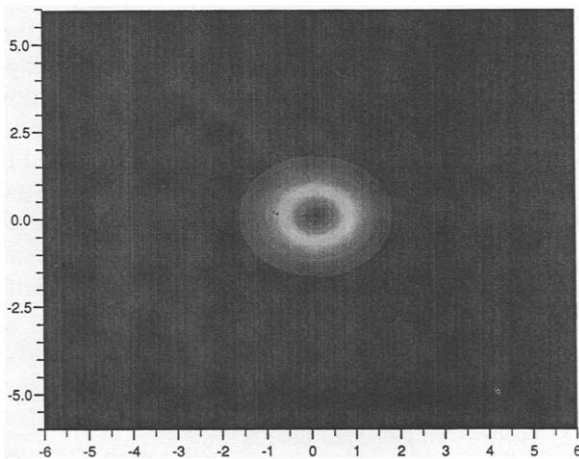


Fig. 1. Intensity profile in the transverse plane (x - y) after linear propagation over a distance $z = 50$. A single phase singularity was seeded at the beam centre which leads to the development of a wide bright ring. ($F_0 = 1, \alpha = 0.002, m = 1$.)

the two-dimensional Fourier transform of the input beam profile.

Figure 2 displays the output after exactly the same initial condition was propagated over the same distance but through a self-defocussing medium. One can see that a well-defined sharp dip in the field persists at beam centre – even while the background beam spreads. This dip has been confirmed to be an absolute zero in the field. In fig. 3a the real part of the complex field is shown revealing that the initially rectilinear defect has “spun” tightly into a spiral, strongly reminiscent of the analogous superfluid phenomenon [12]. In fig. 3b we show the the same simulation except that here a topological charge of “+3” was seeded. In our range of simulations in which single phase singularities were seeded on smooth gaussian beams we have not observed any appreciable break-up of the multiply charged defects into structures of unit charge. There may well be break-up after much longer propagation distances.

To seed a singularity initially off beam centre (off-axis), say at $\mathbf{r} = (r_0, \phi_0)$, we let $\mathbf{r} \rightarrow \mathbf{r} - \mathbf{r}_0$ for the singularity characteristics in the type of initial condition defined by eq. (2). For $m = 1$ we can write this as the following simple linear superposition,

$$F(r, \theta, z=0) = F_0 \exp(-r^2) \times [r \exp(i\theta) - r_0 \exp(i\phi_0)]. \quad (3)$$

Full simulations show the same essential features

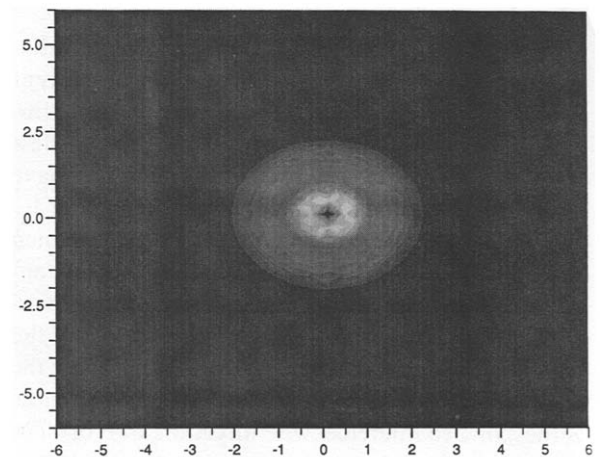


Fig. 2. Output intensity after propagation through a self-defocussing medium – other parameters as in fig. 1.

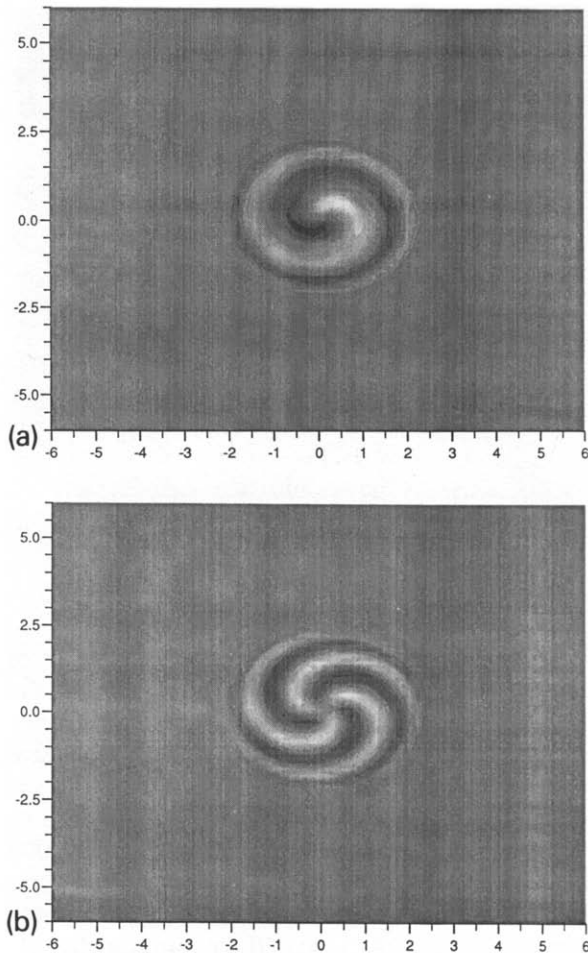


Fig. 3. Spiral developments in the phase after a rectilinear singularity was seeded at $z=0$. (a) $m=1$, (b) $m=3$ – other parameters as in fig. 1.

present in the on-axis cases. This is quite an impressive robustness of the vortex when compared with the propagation of an off-axis dark “soliton stripe” [7]. We return to off-axis propagation in more detail in the last section of this paper.

3. Evolution on plane wave background

To accurately extend the duration of the earlier gaussian beam simulations one would, most preferably, use a self-adjusting spatial grid which could capture both the local vortex structure and the widely

diffracted and defocussed background beam. As an exploration into some of the features of vortex dynamics over much longer propagation distances we now reduce the problem to consideration of evolution on a plane wave background. In this case, numerical simulation is simplified by adopting spatially periodic boundary conditions whereby the computational grid becomes the unit cell of a spatially periodic lattice. This problem may relate to wide beams containing many vortices and should give insight into the robustness, interactions and stabilisation of any vortex ensembles which may form.

To define a phase singularity in the plane, we choose an initial field profile for which any straight line passing through the defect core may locally reproduce the shape of a dark soliton. We thus consider

$$F(r_1, \theta_1, z=0) = F_0 \tanh(r_1/r_w) \exp(im\theta_1). \quad (4)$$

r_w is a width parameter and (r_1, θ_1) are the polar coordinates relative to the position of the defect core. Since we do not consider infinitely distant spatial boundaries, lines of phase discontinuity will be present along with the defined point defects.

We would limit ourselves if only one point of singularity were to be defined. We thus consider separate regions of the transverse plane where singularities are locally defined. Here we shall report only on the case of four initial singular points, each having been defined separately in one of the four quadrants of the transverse plane. The intensity profile arising from such an initial condition is shown in fig. 4. Here no information is present to indicate what topological charges are involved. To display information about the phase one can plot points in the transverse plane where either the real or imaginary part of the field passes through zero. This collection of points are a sample of continuous lines (the “phase lines”) and the monitoring of these lines provides insight into the topology of the phase dynamics.

In fig. 5 the phase lines are shown after a “++++” pattern has been allowed to propagate a short distance. Prior to break-up into vortices, the initial effect of nonlinear propagation on the line discontinuities is to modulate the plane background intensity profile forming dark lines. Each quadrant in the transverse plane has essentially the same pattern. In each, the initial vortex is relatively well developed and dominates. The creation of new vortices is has-

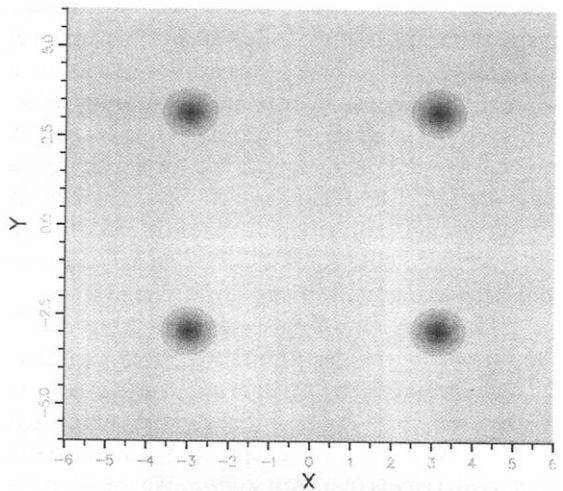


Fig. 4. Initial transverse intensity profile of four singularities on a plane wave background.

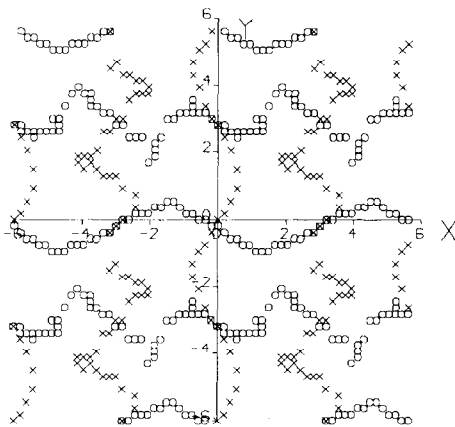


Fig. 5. Break-up of the lines of phase discontinuity ($x = -6, 0, 6$; $y = -6, 0, 6$) leading to the creation of additional vortices. Points where either the real or imaginary part of the field is zero are marked with symbols. ($F_0 = 1, \alpha = 0.03, r_w = 0.3, z = 3.$)

tened by the attempts of each initial vortex to develop a spiral phase pattern. At this stage in the evolution the pattern in each quadrant is highly reminiscent of the simulations of ref. [9]. However, here propagation evolves the system to allow each vortex to be on an equal footing. In fig. 6 the intensity profile at $z = 1000$ is shown which is a square lattice pattern of 16 optical vortices. This pattern has already stably persisted in the system over a distance of more than $\Delta z = 800$. We stress that, unlike the sta-

FIGURE EIGHT
Fig. 8

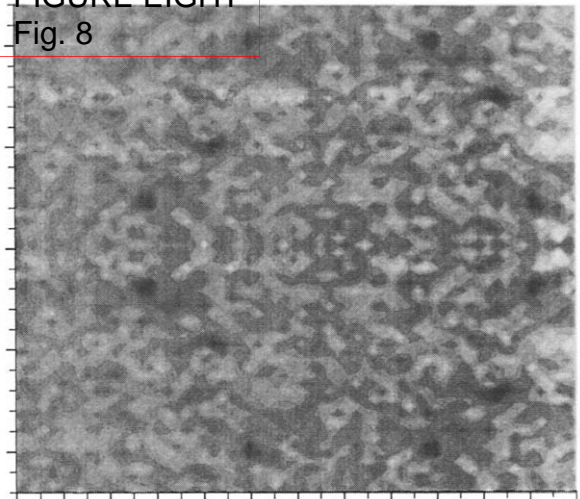


Fig. 6. Intensity profile of a vortex crystal pattern in the transverse plane ($z = 1000$, x and y both extend from -6 to $+6$).

tionary crystal of phase singularities in ref. [11], we report here the stabilisation to crystal structure of (fully nonlinear) vortices without restriction to the modelling of a finite number of transverse modes.

From consideration of only the isolated plane wave background solution, the phase lines themselves cannot here adopt a stationary pattern. In fig. 7 we show snapshots of the phase lines at $z = 800, 900$ and 1000 illustrating the regular patterns that they cycle through. Considering the incremental effect of only the nonlinearity of the 3D NLS on an initially rectilinear singularity at $z = z'$: $F(r, \theta, z') = \tanh(r) \exp(i\theta)$, we can write

$$F(r, \theta, z' + \delta z) = \exp[i\eta |\tanh(r)|^2 \delta z] F(r, \theta, z') \quad (5)$$

The vortex core ($r = 0$) experiences no nonlinear phase shift and in this sense is actually linear. However the sharp intensity gradient in the neighbourhood of the core implies a rapid change of phase, which results in a rotation of the phase lines in full propagation. This configuration of phase lines does not persist indefinitely as the lines are continuous across the plane. Instead both the real and imaginary phase lines meet up with others of the same kind, break their original pattern and form new transient loops. With the above considerations, this new pattern will also be short lived as the vortices persist in

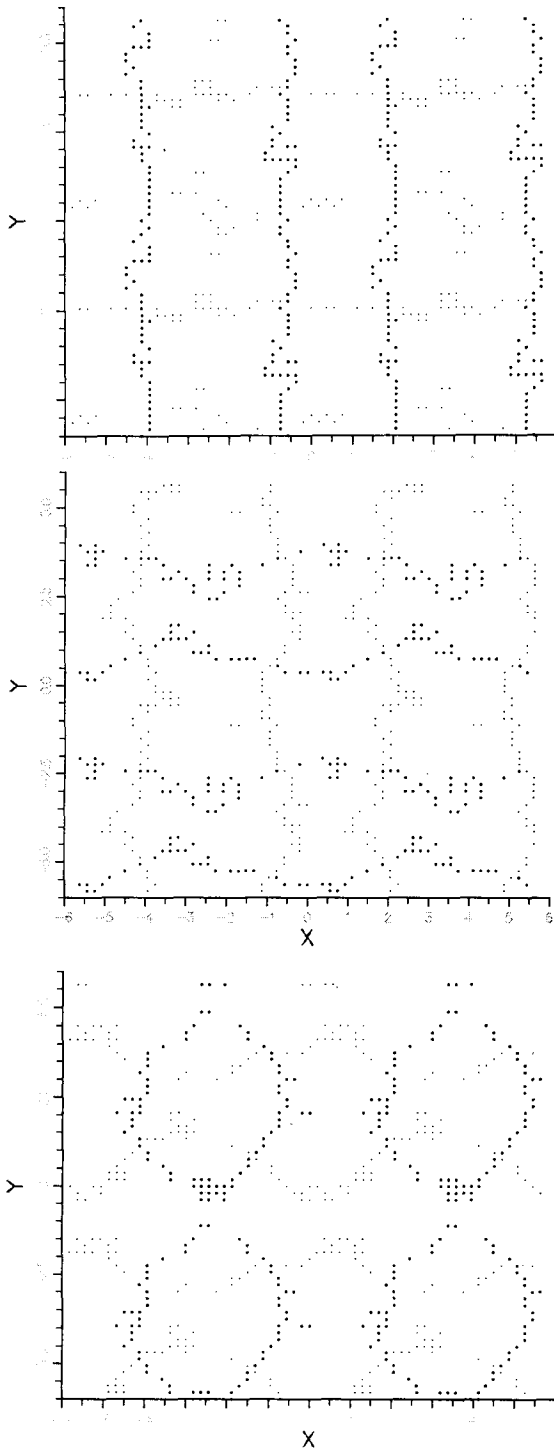


Fig. 7. Snapshots of the underlying phase evolution and phase line interchanging while the intensity maintains a regular vortex array. $z =$ (a) 800, (b) 900, (c) 1000.

rotation. After the lines once again touch their neighbours of the same type, they again break and exchange the lines of continuity and the transition between, for example the configurations shown in figs. 7a and 7b, is complete. Note that this can occur while maintaining the overall topological charge (no creation or annihilation of vortices) and also sustaining the vortex crystal. The phase lines appear to pass through this cycle endlessly but the exact overall position of the vortex crystal may shift slightly.

Defects have been seen to mediate the transition from an ordered to disordered system [13] but here we can see that, as with the linear defects of Brambilla et al. [11], they can in fact stabilise into regular crystal lattices. Indeed, in our case, the transition from disordered to ordered would seem more appropriate.

Starting from a different initial condition the system may instead remain, over very long propagation distances, in a seemingly turbulent state. Figure 8 corresponds to exactly the same set of parameters as those of figs. 4–7. Here the initial condition again arose from the definition of four square zones in the plane each with a central point singularity. However, in this case the overall topological configuration was “+ - + -” where zones defining unlike charges shared common boundaries. Although this unsettled pattern resembles a vortex gas there is a preserved

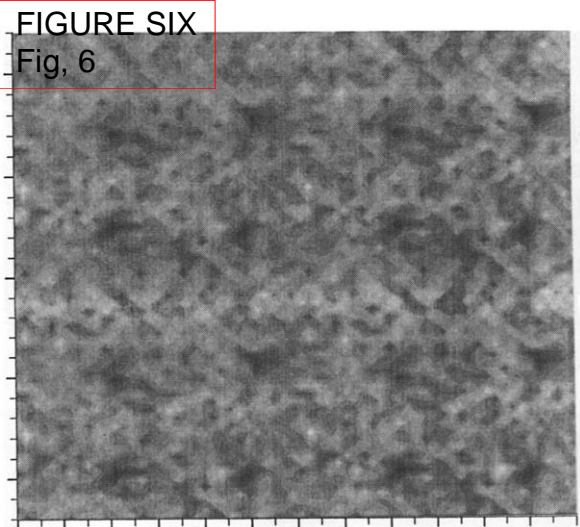


Fig. 8. Vortex gas-like structure at $z = 1000$. Parameters are those of figs. 4–7 except that a different initial condition is defined.

symmetry (reflection about $y=0$) and the pattern is constrained as it evolves. In this (2+1)D system vortices interact through their phase lines touching and certainly dominate the evolution but move in a direction parallel to the x axis.

4. Equations of vortex motion

A central consideration in real systems is the understanding of any motion of an initially off-axis vortex due to a modulated (gaussian) background and beam expansion. A change in the radial position of the vortex may be intuitively expected as the beam widens. However, in fig. 9, we explicitly demonstrate also *rotation* of an off-axis vortex around beam centre. We have discovered that in the early stages of linear propagation the (initially singular) ‘‘hole’’ also rotates and to a greater extent than during propagation through our defocussing medium (α fixed, $\eta=0, -1$). The amount of rotation in the defocussing case was seen to depend on the initial position of the defect on the beam, but such a dependency was not observed in linear propagation.

To capture the vortex dynamics quantitatively, we can use our prior knowledge gained from full simulations to guess a trial solution for a variational approach. Specifically, we have chosen a trial solution of the form

$$F(x, y, z) = F_0 \exp[-\gamma(x^2 + y^2)] \times [x - x_0 + i(y - y_0)] \tag{6}$$

where both F_0 and γ are allowed to be complex functions of z . We separate γ into its real and imaginary parts (γ_r and γ_i) whereby the real part implies the gaussian beam waist. The 3D NLS may be written in the form of an Euler–Lagrange equation, $\partial L / \partial F^* = 0$ with lagrangian

$$L = \frac{1}{2} \left[\alpha |\nabla F|^2 - i \left(\frac{\partial F}{\partial z} F^* - F \frac{\partial F^*}{\partial z} - \eta |F|^4 \right) \right] \tag{7}$$

where F^* denotes the complex conjugate of the field.

Upon substitution of (6) into (7) and integrating out the transverse dependence we find a form for the lagrangian in terms of only z and the parameters of solution (6). Calculation of the Euler–Lagrange equations yield, after simplification, the following

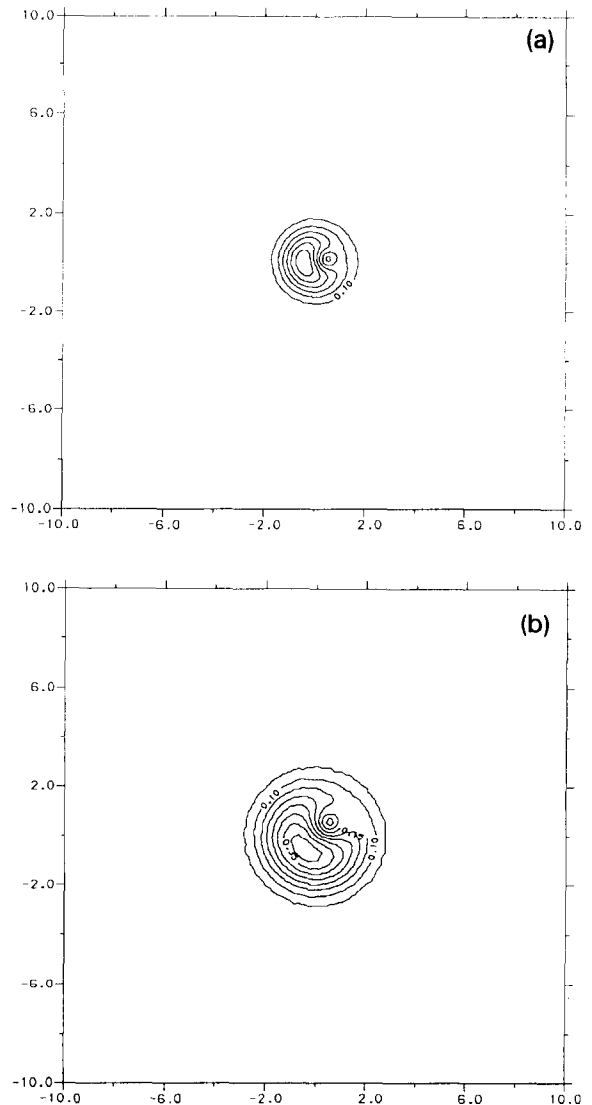


Fig. 9. Off-axis vortex rotating around beam centre. $z =$ (a) 0.1, (b) 0.6. ($F_0=1, \alpha=1, m=1, r_0(z=0)=0.4.$)

simple set of evolution equations for the parameters. Firstly, as in linear beam propagation with or without a defect, one has equations governing the width and height of the beam:

$$d\gamma_r/dz = 4\alpha\gamma_r\gamma_i \tag{8}$$

$$d|F_0|/dz = 4\alpha|F_0|\gamma_i \tag{9}$$

where vortex position has been expressed in polar form (r_0, ϕ). The beam phase and rotation of the

vortex have both linear and nonlinear contributions:

$$\frac{d\gamma_r}{dz} = 2\alpha(\gamma_i^2 - \gamma_r^2) + \eta|F_0|^2 \left(\frac{\gamma_r r_0^2}{2} + \frac{1}{16(1 + \gamma_r r_0^2)} \right), \quad (10)$$

$$\frac{d\phi}{dz} = 2\alpha\gamma_r + \eta|F_0|^2 \left(\frac{1}{8\gamma_r} + \frac{\gamma_r r_0^2}{2} + \frac{1}{16(1 + \gamma_r r_0^2)} \right). \quad (11)$$

Finally, a remarkably simple constraint governing beam width and intensity and the vortex position is found:

$$|F_0|^2 r_0^2 / \gamma_r = \text{const.} \quad (12)$$

The qualitative observations made earlier are predicted by the above system equations. From (8) and (9) it is obvious that $|F_0|^2$ decays faster than γ_r and thus the constraint (12) implies that r_0 will increase as the beam spreads. In linear propagation, while the trial solution remains a reasonable approximation, the rotation of the dark spot loses its complicated dependence on position. Also, the rotation of the vortex can be slowed by the defocussing nonlinearity.

For a quantitative comparison, we have solved the system (8)–(12) numerically using a simple fourth order Runge–Kutta algorithm. A wide range of initial conditions have been tested and compared with full 3D simulations. Excellent agreement has been found and, in fig. 9, we highlight vortex evolution on a relatively narrow beam ($\alpha = 1$). This leads to large diffractive spreading and fully tests the predicted interplay between vortex and gaussian beam parameters. In fig. 10a the evolution of the vortex position in terms of the distance from the beam centre, r_0 , is shown. Here both analysis and full simulation show good agreement over a propagation distance such that r_0 doubles. In fig. 10b predictions of the angular position of the vortex, ϕ , are also ratified. Both r_0 and ϕ for the simulations are derived from estimations of the (x, y) position of the vortex. Data discretisation leads to finite uncertainties in the polar coordinates which are greatest for angles in the case of small r_0 . We stress that agreement may continue to higher z but that we are constrained, as outlined earlier, by beam expansion and the numerical scheme adopted.

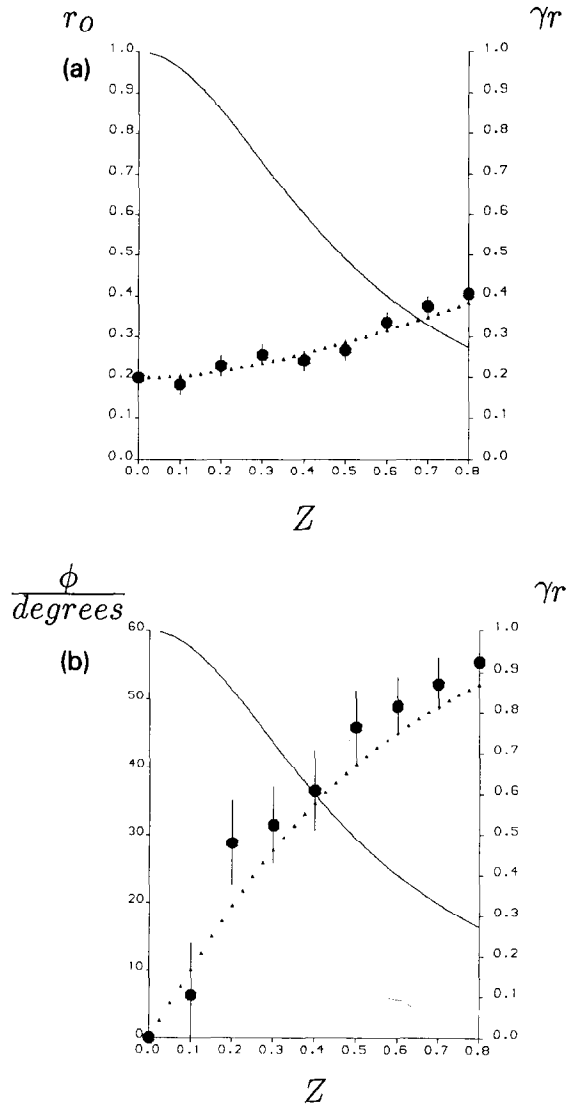


Fig. 10. Comparison of theory and full simulation. Solid curves give the evolution of the beam size parameter, γ_r . Values from analysis are shown with broken curves while measured values (and their uncertainties) are plotted with large dots (and error bars). (a) Vortex distance from the beam centre; (b) angular coordinate of the vortex. ($F_0 = 1, \alpha = 1, m = 1$.)

5. Conclusions

On plane wave background we have discovered both vortex gas-like solutions and stabilisation into regular crystals of fully nonlinear vortices. We have also demonstrated and explained the topology of the

phase line interactions which allow the formation of these crystals.

A simple set of ordinary differential equations governing the evolution of a vortex, including finite beam effects, has been derived and excellent agreement has been obtained between this reduced system and the full 3D simulations.

Optical vortices appear to be stable in many passive and active systems. The results presented here underpin current and future studies of their role in higher-order systems where cavities, laser gain and other effects are taken into consideration.

Since the vortex appears to be a robust structure in so many 3D optical systems, it is interesting to speculate on their possible utilisation in information processing. Such operations as the selection or "pinning" of single vortex or pattern of vortices, maybe in an analogous manner to that of spatial solitons [14], to effect a memory device or vortex coding in a transmission system may be conceived.

Acknowledgements

The authors would like to acknowledge useful discussions with Ewan M. Wright, Gian-Luca Oppo and Gianpaolo D'Alessandro. This work is supported in

part by Science and Engineering Council Grants Nos. GR/F 76502 and GR/G 12665, and in part by a Twinning contract of the European Communities.

References

- [1] N.B. Abraham and W.J. Firth, *J. Opt. Soc. Am. B* 7 (1990) 951 and *op. cit.*
- [2] R.Y. Chiao, E. Garmire and C.H. Townes, *Phys. Rev. Lett.* 13 (1964) 479.
- [3] G.A. Swartzlander Jr., D.R. Anderson, J.J. Regan, H. Yin and A.E. Kaplan, *Phys. Rev. Lett.* 66 (1991) 1583.
- [4] D.R. Anderson, D.E. Hooten, Grover A. Swartzlander Jr. and A.E. Kaplan, *Optics Lett.* 15 (1990) 783.
- [5] G.R. Allan, S.R. Skinner, D.R. Andersen and A.L. Smirl, *Optics Lett.* 16 (1991) 156.
- [6] V.E. Zakarov and A.B. Shabat, *Sov. Phys. JETP* 37 (1973) 823.
- [7] G.S. McDonald, K.S. Syed and W.J. Firth, *Optics Comm.*, submitted.
- [8] A.L. Fetter, *Phys. Rev.* 151 (1966) 100.
- [9] P. Coullet, L. Gil and F. Roca, *Optics Comm.* 73 (1989) 403.
- [10] G.-L. Oppo, G. D'Alessandro and W.J. Firth, *Phys. Rev. A* 44 (1991) 4712.
- [11] M. Brambilla, F. Battipede, L.A. Lugiato, V. Penna, F. Prati, C. Tamm and C.O. Weiss, *Phys. Rev. A* 43 (1991) 5090.
- [12] E.B. Sonin, *Rev. Mod. Phys.* 59 (1987) 87.
- [13] P. Coullet, L. Gil and J. Lega, *Physica D* 37 (1989) 91.
- [14] G.S. McDonald and W.J. Firth, *J. Opt. Soc. Am. B* 7 (1990) 1328.